

Examination of Fatigue Crack Origins in Aircraft Turbine Blades Using Serial Sectioning Techniques

Sylvie Dionne¹, Tim Lang¹, Jian Li²

¹*Transportation Safety Board of Canada, Ottawa, Canada;* ²*CANMET-Materials Technology Laboratory, Ottawa, Canada*

1. Abstract

Fatigue cracking of aircraft engine turbine components can initiate at metallurgical defects that were not detectable during post-manufacturing inspections. This paper presents the results obtained during the detailed metallurgical examination of turbine blades from recently completed accident investigations. The subject blades were examined in a scanning electron microscope operated in the topographic mode to pinpoint the location of the fatigue origins. Serial sectioning was then performed to characterize the blade microstructure at the suspected fatigue crack origins. In one case, a focused ion beam instrument was employed to examine several potential origins while minimizing damage to the rest of the fracture face. The fatigue crack origins were identified as casting-related defects. The conditions under which such defects could be detected using non destructive inspection techniques are discussed.

2. Introduction

The major causes of component failures in modern aircraft turbine engines include high cycle fatigue, low cycle fatigue, corrosion, overstress, manufacturing processes and materials [1]. Amongst these causes, inherent material defects such as metallurgical and machining anomalies are relatively rare. However, metallurgical defects such as inclusions and voids are well known to reduce the fatigue life of superalloy turbine components and can have a significant impact on component reliability. The inclusions and voids produce microscopic stress concentrations under load due to the difference in modulus with respect to the parent material [2]. This can result in premature initiation of slip, and eventually develop into fatigue microcracks. Internal discontinuities such as oxide skins and seams can also act as fatigue crack origins. Probabilistic fatigue life analysis techniques such as the damage tolerance process specified in FAA Advisory Circular (AC) 33.14-1 have been developed to mitigate the risks associated with material anomalies [3]. An understanding of the defect size, occurrence and probability of detection is critical to this damage tolerance process. The examination of failed components can provide valuable information concerning defects that were missed during the post-manufacturing inspections.

In most cases, the suspected origin of a fatigue failure can be identified by using standard fractographic techniques based on optical and scanning electron microscopy equipment. However, it is often necessary to examine the underlying

¹ E-mail: Sylvie.Dionne@tsb.gc.ca

microstructure in a precise location on the fracture face to determine the metallurgical reason for fatigue crack initiation. Conventional sectioning techniques are suitable for this purpose but there is a significant risk of missing small areas of interest. Furthermore, the conventional techniques are destructive and can damage the fracture face so that further examination is no longer possible. In recent years, the focused-ion-beam (FIB) microscope has emerged as a powerful tool for failure analysis of engineering components [4]. The FIB instrument uses a focused beam of gallium ions to mill out site-specific cross-sections while minimizing damage to the remainder of the fracture face. Prior to FIB sectioning, a thin layer of tungsten is deposited on the area of interest to prevent damage to the surface features. High-resolution FIB images of the cross-sections are obtained by tilting the sample.

This paper presents the results obtained using FIB and conventional serial sectioning techniques to identify metallurgical defects at suspected fatigue crack origins in aircraft turbine blades.

3. Examination and Results

3.1. Compressor Turbine Blade

A compressor turbine (CT) failure was identified as the primary cause of the in-flight failure of an aircraft engine. Visual examination of the CT wheel determined that all of the blades had fractured in an instantaneous overstress mode of failure except for one blade which showed a progressive mode of failure. This CT blade had fractured close to the platform (Figure 1). The trailing portion of the subject blade fracture face exhibited a flat faceted topography consistent with fatigue failure (Figure 2) while coarse fibrous features consistent with overstress (Figure 3) were observed in the leading portion. The subject blade was examined in a scanning electron microscope (SEM) using a quadrant type semiconductor back scattered electron (BSE) detector operated in the topographical mode. Based on the orientation of fatigue beach marks observed on the BSE images, it was determined that fatigue cracking initiated near the trailing edge (Figure 2) and progressed towards the leading edge in a high cycle mode until the blade eventually separated by overstress extension of the high cycle fatigue cracking.

FIB cross-sections were prepared from the subject CT blade to determine if any metallurgical anomalies were associated with the suspected fatigue origin. Figure 4 shows the location of three FIB sections prepared in the trailing portion of the CT blade. The first FIB section was made to examine the bond between the coating and blade parent material on the pressure side of the blade near the trailing edge (Figure 5). The FIB section showed a few small pores at the interfaces between the aluminide layer, diffusion zone and blade parent material. These pores were considered to be typical of diffusion-processed coatings. No evidence of cracking or coating failure was observed. A narrow band of

topologically closed-packed (TCP) phases was observed in the blade material adjacent to the diffusion zone. It was determined that the band of TCP phases was a normal feature of CT blades subjected to a similar time in service.

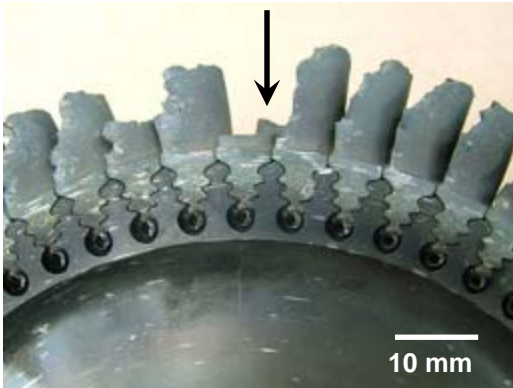


Figure 1: Photograph showing the subject CT blade in-situ (arrowed, trailing edge view).

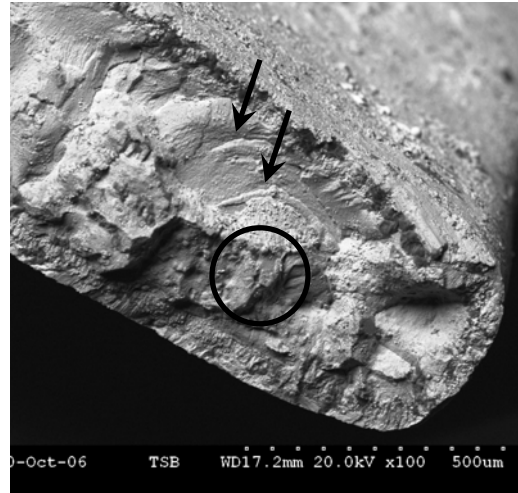


Figure 2: BSE image of the trailing portion of the CT blade fracture face showing beach marks (arrows) and the suspected fatigue crack origin (circled).

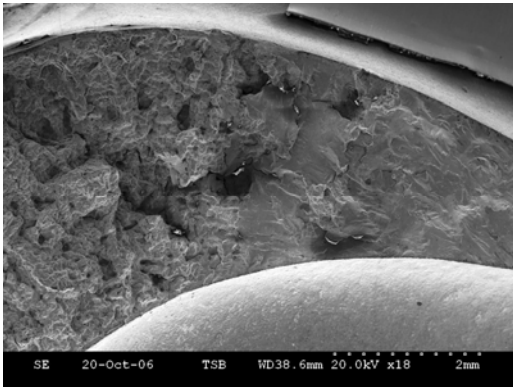


Figure 3: SEM image of the CT blade fracture face showing the transition from fatigue (left) to overstress (right) regions.

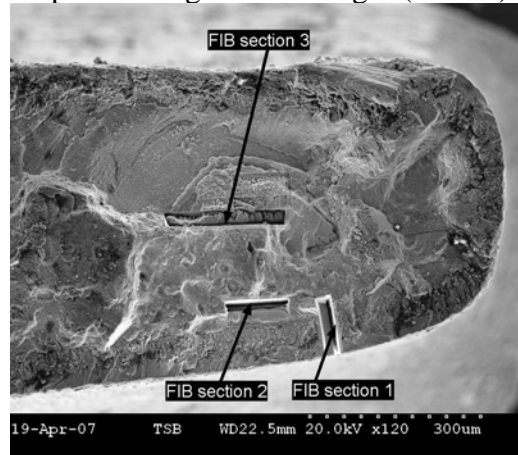


Figure 4: SEM image of the trailing portion of the CT blade fracture face showing the three FIB sections.

The second and third FIB sections were taken across a region with a rounded dendrite-like appearance on the fracture face (Figure 4). These FIB sections revealed the presence of seams extending into the blade material below the fracture face (Figure 6). The seams had a complex structure consisting of multiple layers and particles (Figure 7). Energy dispersive spectroscopy (EDS) analysis showed that the seams were oxygen-rich (Figure 8). These observations suggested that there was an anomaly with similar characteristics to those of an internal casting pore at the origin of the fatigue crack on the subject CT blade.

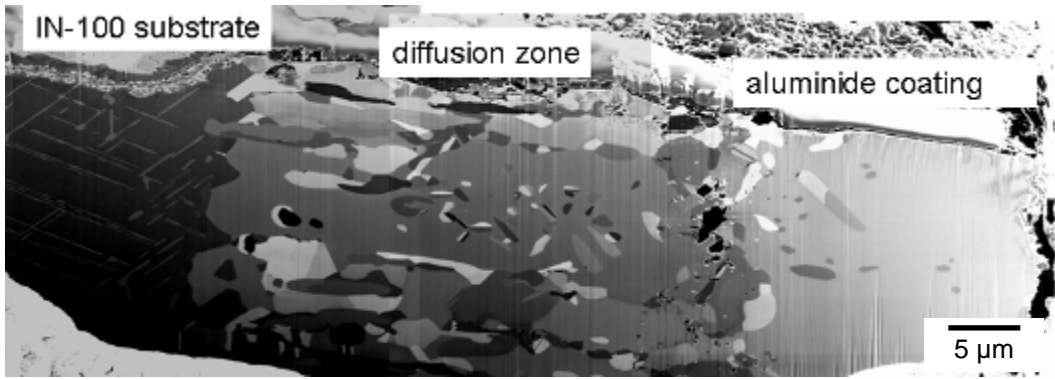


Figure 5: Montage of FIB images of FIB section 1 showing the coating, diffusion zone and blade material in the vicinity of the suspected fatigue crack origin.

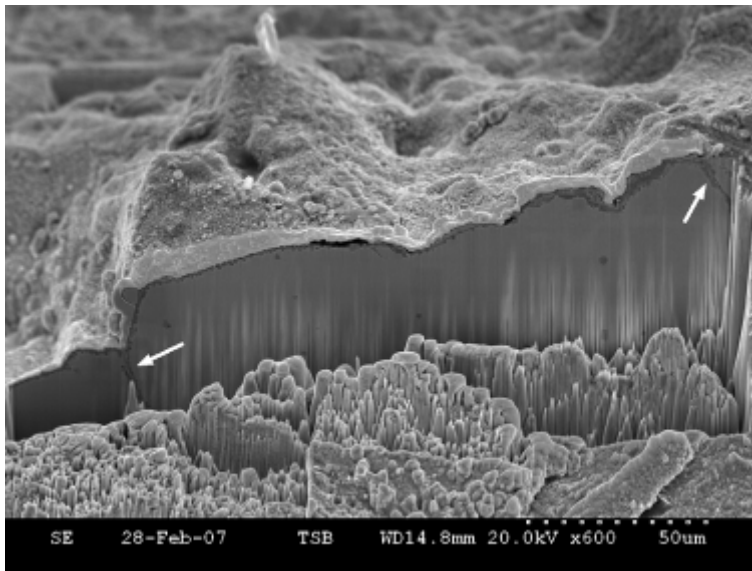


Figure 6: SEM image of FIB section 3 showing seams (arrowed).

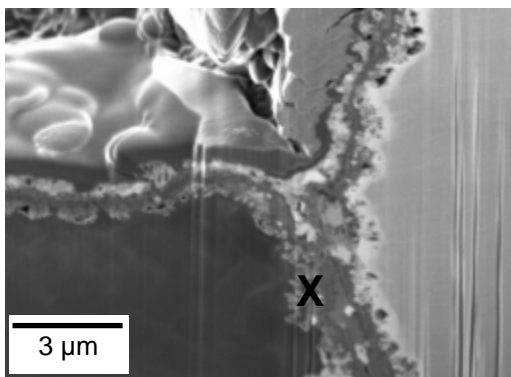


Figure 7: FIB image showing the left seam arrowed on Figure 6.

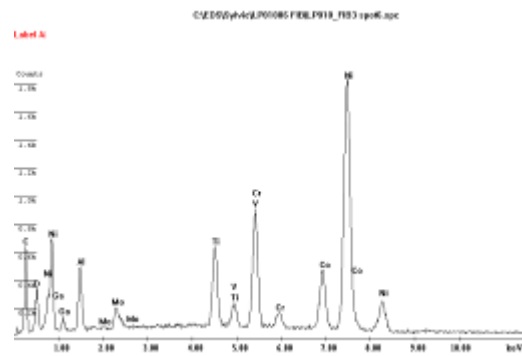


Figure 8: EDS spectrum obtained from the location marked on Figure 7.

Conventional metallurgical sections were prepared from the subject blade to determine the size of the region affected by the seam defects. The blade was mounted in transparent cold setting epoxy and sectioned using a tool capable of controlled material removal in increments of 20 microns (Figure 9). Section polishing was accomplished using conventional metallographic preparation techniques. In total, twenty-five polishing steps were completed to document the microstructure in the trailing portion of the blade. The location of each plane of polish was determined using features on the fracture profile and the FIB sections as reference points. Figure 10 shows the position of the plane of polish after the 8th (line A, 400 μm from the blade trailing edge) and 23rd (line B, 910 μm from the blade trailing edge) polishing steps, respectively.

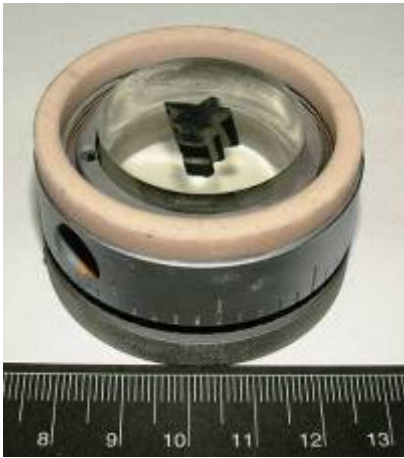


Figure 9: Controlled material removal tool employed for preparation of blade metallurgical sections.

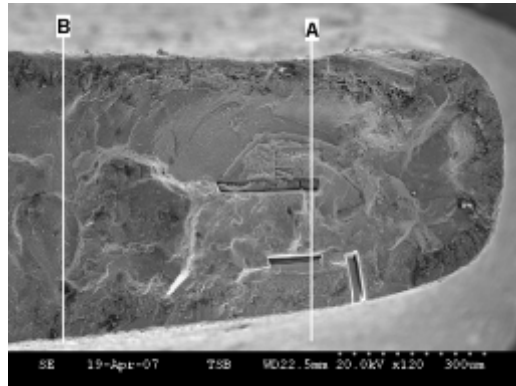


Figure 10: SEM image of the trailing portion of the subject CT blade showing the location of two metallurgical sections (lines A and B).

Polishing steps one through seven revealed a typical cast superalloy microstructure with a well defined gamma prime phase. The uniform distribution of the gamma prime phase indicated that the blade had not been exposed to excessively high temperatures. Semi-quantitative standard less EDS analysis showed that the blade material was in agreement with the compositional requirements for the major elements of the cast IN-100 alloy specified for the blade. At the 8th polishing step, a large cluster of seams was observed adjacent to the fracture face (Figure 11). EDS elemental mapping showed that the center of the seam defects was nickel-rich while the outer layers contained oxygen, aluminum, titanium and chromium (Figure 12). Polishing steps nine through twenty-four showed that the seams formed a continuous network. In several locations the fracture face was coincident with a seam, suggesting that the blade had separated at the seam. Secondary cracks and small pores associated with the seams were also observed (Figure 13). The seams had essentially disappeared by the 25th polishing step, corresponding to a location approximately 2 mm from the trailing edge. The size of the seam cluster was estimated at approximately 1 mm in overall length, coincident with the fatigue cracking origin observed on the fracture face.

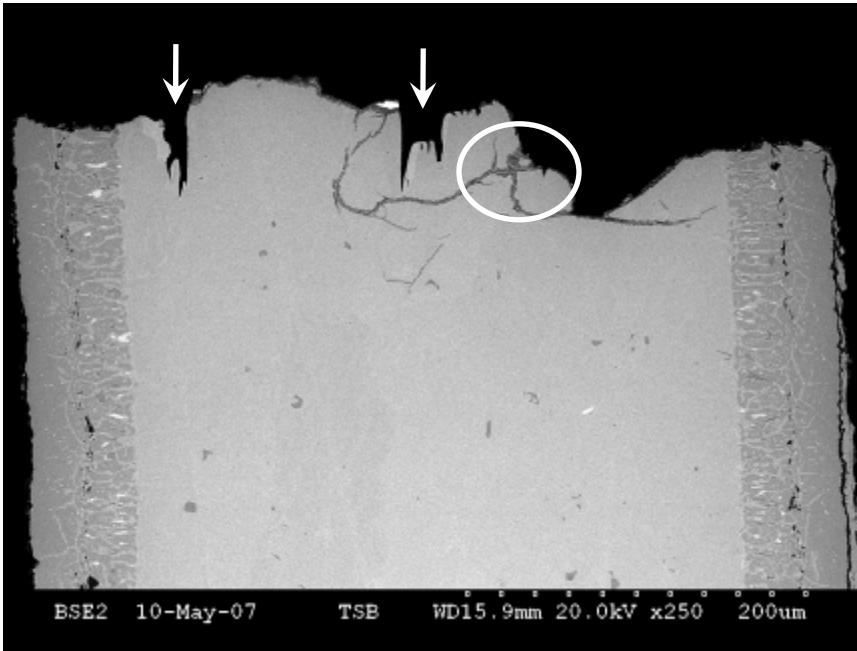


Figure 11: SEM image of a cross-section of the subject CT blade after the 8th polishing step (refer to line A on Figure 10). Arrows point to the location of FIB sections 2 (left) and 3 (right).

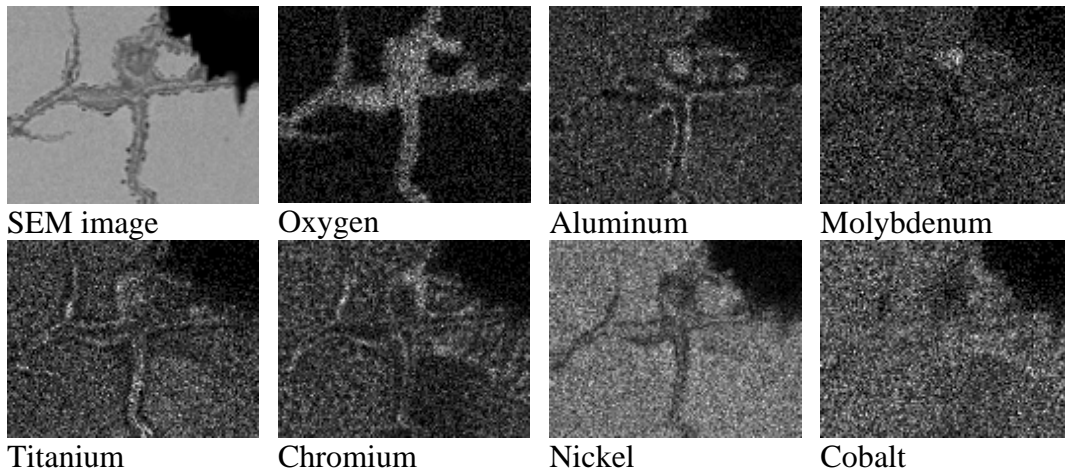


Figure 12: SEM image and associated EDS elemental maps showing the distribution of elements in a cluster of seam defects (refer to the area circled on Figure 11).

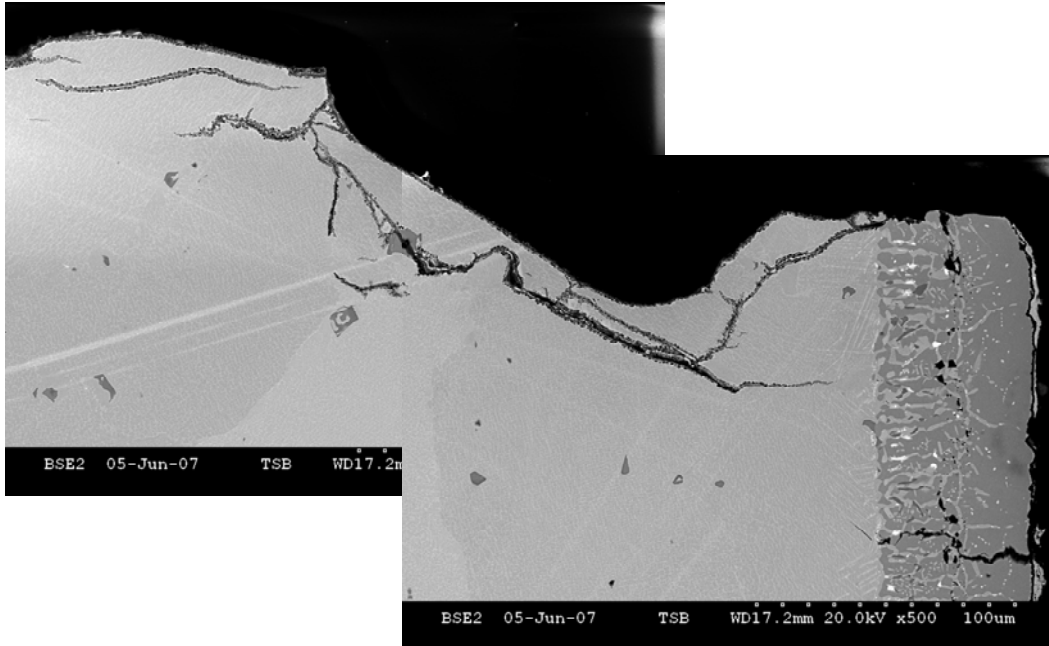


Figure 13: Montage of SEM images of a cross-section of the subject CT blade after the 23rd polishing step (refer to line B on Figure 10) showing seam defects associated with the fracture face and internal cracks.

3.2 Third stage turbine wheel

The examination of a helicopter engine that had sustained an in-flight loss of power showed that three blades had separated from the third stage turbine wheel. One blade had separated at mid-span and contained a region of flat faceted fracture consistent with a progressive mode of failure (Figure 14). The region of progressive failure was tarnished, indicating that the crack had been exposed to the environment for some time before blade separation. The two other blades had separated a few millimeters from the shroud and their fracture faces had a fibrous appearance typically associated with failure due to overstress. Rub damage was observed on the seal and shroud opposite the separated blades consistent with unbalanced operation of the wheel resulting from blade separation.

Figure 15 is a BSE image of the progressive failure region on the subject third stage turbine blade. Based on the direction of local crack propagation deduced from the orientation of the beach marks, the origin of the fatigue crack was a region with a dark contrast at the leading edge of the blade. Fatigue striations were faintly visible at higher magnification but oxidation of the fracture face precluded the determination of striation spacing. The suspected fatigue crack origin had a granular texture and contained several secondary cracks. EDS elemental mapping revealed the presence of oxygen, magnesium, aluminum and silicon enrichments in varying concentrations throughout the region of fatigue crack initiation.

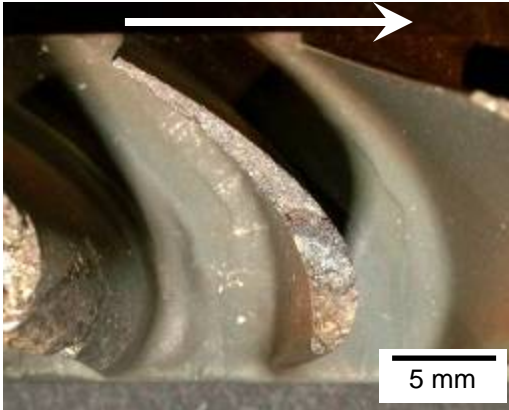


Figure 14: Photograph showing the subject third stage turbine blade. An arrow indicates the direction of rotation.

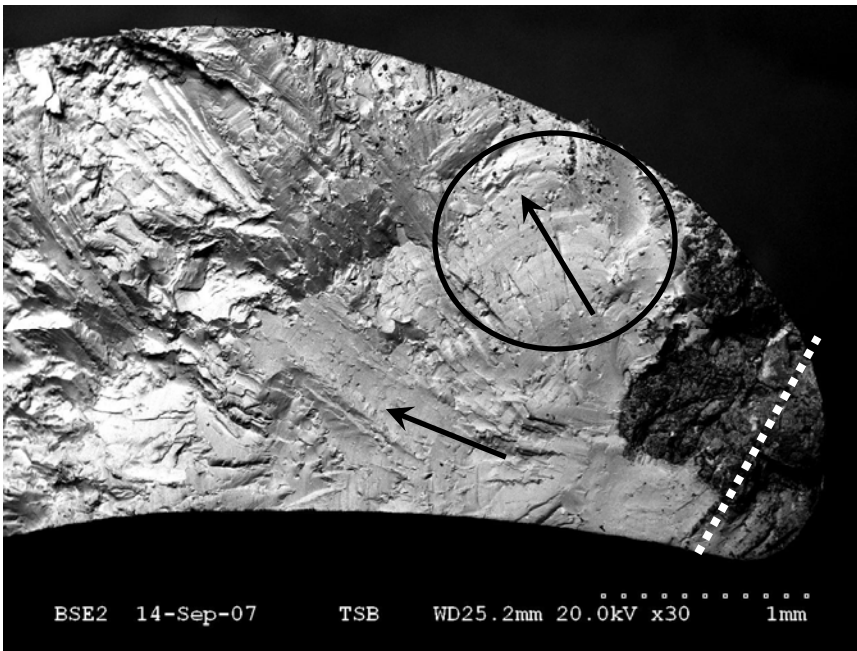


Figure 15: BSE image of the progressive failure region on the subject third stage turbine blade. A region containing beach marks is circled.

A metallographic cross-section was prepared from the subject third stage turbine blade using the serial sectioning technique described previously to determine the depth of the fatigue crack origin in the axial direction. The location of the plane of polish is indicated by a dashed line on Figure 15. Figure 16 is a montage of BSE images showing that the fatigue crack origin was composed of a network of small pores and seams with a darker contrast than the blade material. These seams were present at the fracture face and along secondary cracks. The secondary cracks and seams extended approximately 50 microns below the fracture face. The films adjacent to a secondary crack were enriched with oxygen, magnesium, aluminum, titanium and chromium in comparison with the blade parent material (Figure 17). Silicon and potassium were also detected in some particles within these films. Semi-quantitative EDS analysis showed that

the third stage turbine blade material was in agreement with the compositional requirements for the major elements of IN-713C.

The appearance and composition of the seams observed at the fatigue crack origin was consistent with a casting-related anomaly. This type of anomaly is observed when impurities (slag) from the top of the molten metal pool in the crucible are carried over into the mold during casting of the blade. Overall, the anomaly covered approximately 1 square millimeter of the fracture face at the leading edge. The microstructure of a comparison blade did not show any evidence of microstructure changes resulting from exposure to excessive temperature. No casting-related anomalies were detected in the comparison blade.



Figure 16: Montage of BSE images showing the central portion of the fracture profile on a metallographic cross-section through the leading portion of the third stage turbine blade (refer to the dashed line on Figure 15).

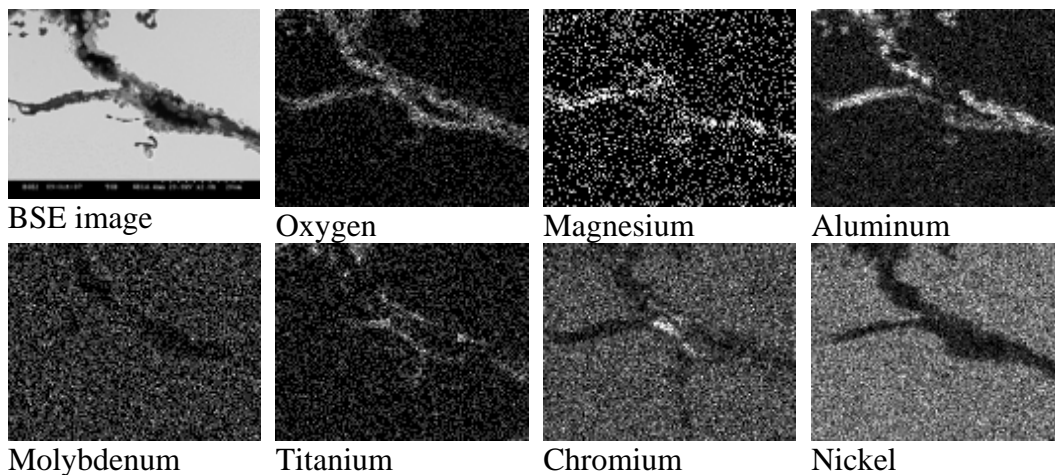


Figure 17: BSE image and associated EDS elemental maps showing the distribution of elements around a secondary crack in the subject third stage turbine blade (refer to the circled area on Figure 16).

4. Analysis

Aircraft turbine blades are inspected using the radiography and liquid penetrant techniques. Radiographic techniques can detect visible surface cracks and internal flaws such as voids and pores. However, seams and minute surface cracks are undetectable by radiography. Liquid penetrant techniques can detect defects as small as 1 mm (0.040 inch) but the defect must be sufficiently open to provide a flow path for the liquid penetrant to wick in. In the present cases, the metallurgical anomalies formed a network of seams and small pores with open sections less than 1 mm in size. Therefore, it is unlikely that these anomalies could have been detected at manufacturing. After some time in service, a fatigue crack initiated at the weak points created by the seams and pores in the defect. The fatigue crack subsequently grew to a size much larger than 1 mm and would have been detectable using liquid penetrant inspection. However based on the observations of the fracture faces, it was not possible to determine at what time in the service life of the blade the fatigue cracks initiated and grew to a detectable size.

5. Conclusions

- Metallurgical defects in turbine blade materials can promote early initiation of fatigue cracks leading to early failure of turbine components.
- FIB and serial sectioning techniques permit a complete characterization of the fatigue failure origin including an estimate of the size of the metallurgical defect.
- Metallurgical defects in the subject turbine blades were identified as casting-related anomalies consisting of seams and small internal pores. These defects were likely undetectable at manufacturing.

6. References

- [1] B. A. Cowles, High Cycle Fatigue in Aircraft Gas Turbines: an Industry Perspective, *International Journal of Fracture* 80 (2-3) (1996) 147-163.
- [2] J. D. Varin, Microstructures and Properties of Superalloys, in C. T. Sims and W. C. Hagel (Eds.), *The Superalloys*, John Wiley & Sons, New York, 1972, pp.231-257.
- [3] Damage Tolerance for High Energy Turbine Rotors, Advisory Circular (AC) 33.14-1, U.S. Dept. of Transportation, Federal Aviation Administration, Washington, DC, 2001.
- [4] J. Li, The Focused-Ion-Beam Microscope – More than a Precision Ion Milling Machine, *JOM* 58 (3) (2006) 27-31.